Journal of
Holography and Speckle
Vol. 5, 1–17, 2009

A Review of Incoherent Digital Fresnel Holography

Joseph Rosen[1,*], Gary Brooker[2], Guy Indebetouw[3], and Natan T. Shaked[1]

[1] *Department of Electrical and Computer Engineering, Ben-Gurion University of the Negev, P.O. Box 653, Beer-Sheva 84105, Israel*
[2] *Johns Hopkins University Microscopy Center, Montgomery County Campus 9605 Medical Center Drive Suite 240, Rockville, MD 20850, USA*
[3] *Department of Physics, Virginia Polytechnic Institute and State University, Blacksburg, Virginia 24061, USA*

REVIEW

We review three different methods of generating digital Fresnel holograms of 3-D real-existing objects illuminated by incoherent light. In the first method, a scanning hologram is generated by a unique scanning system in which Fresnel zone plates (FZP) are created by a homodyne rather than the common heterodyne interferometer. During the scanning, the FZP projected on the observed object is frozen rather than varied as previously. In each scanning period, the system produces an on-axis Fresnel hologram. The twin image problem is solved by a linear combination of at least three holograms taken with three FZPs with different phase values. The second hologram reviewed here is the digital incoherent modified Fresnel hologram. To calculate this hologram, multiple-viewpoint projections of the 3-D scene are acquired, and a Fresnel hologram of the 3-D scene is directly computed from these projections. This method enables to obtain digital holograms by using a simple digital camera, which operates under regular light conditions. The last digital hologram reviewed here is the Fresnel incoherent correlation hologram. In this motionless holographic technique, light is reflected from the 3-D scene, propagates through a diffractive optical element (DOE), and is recorded by a digital camera. Three holograms are recorded sequentially, each for a different phase factor of the DOE. The three holograms are superposed in the computer, such that the result is a complex-valued Fresnel hologram that does not contain a twin image.

Keywords:

CONTENTS

1. INTRODUCTION

Holographic imaging offers a reliable and fast method to capture the complete 3-D information of the scene from a single perspective. Commonly, there are two phases in the process of holography, namely, the hologram generation and its reconstruction. Usually in the first phase, light from an object is recorded on a certain holographic medium, whereas in the second phase, an image is reconstructed from the hologram in front of the viewer's eyes. The interaction between holography and the digital world of computers can take place in both phases; in the object acquisition and in the image reconstruction. The mutual relations between the digital computer world and optics in context of holography are illustrated in Figure 1. Basically, there are two methods to generate a hologram, optically or by a computer, as well as there are two methods to reconstruct an image from a hologram, optically or by a computer. The term computer-generated hologram[1] is usually used to indicate the hybrid method in which a hologram is synthesized from computer-generated objects but the reconstruction of the hologram is carried out optically. The term digital hologram[2] (sometimes called electronic hologram) specifies the other hybrid option, in which the hologram is generated optically from real-world objects, then digitally processed and reconstructed in the computer. Therefore, in this review the term incoherent digital hologram (IDH) means that real existing objects illuminated incoherently are recorded or acquired by some electronic detection device, and the detected signals are

*Author to whom correspondence should be addressed.

digitally processed to yield a hologram. This hologram is reconstructed in the computer, whereas 3-D images appear on the computer's screen. The coherent optical recording setup shown in the upper-right corner of Figure 1 is not applicable for the incoherent optics because interference between reference and object incoherent beams cannot occur. Therefore, different holographic acquisition methods should be employed for generating an IDH.

This review concentrates on three techniques of incoherent digital holography that we have recently developed.[3–7] These three methods are different from each other and they are based on different physical principles. There are

Joseph Rosen received his B.Sc., M.Sc., and D.Sc. degrees in electrical engineering from the Technion-Israel Institute of Technology in 1984, 1987, and 1992, respectively. He is currently a professor in the Department of Electrical and Computer Engineering, Ben-Gurion University of the Negev. He is a fellow of the Optical Society of America and has coauthored more than 70 scientific papers in refereed journals. His research interests include image processing, holography, diffractive optics, interferometry, pattern recognition, optical computing, and statistical optics.

Gary Brooker is research professor of chemistry and engineering at Johns Hopkins University in Rockville, Maryland, USA. He obtained his Ph.D. in Pharmacology in 1968 at the University of Southern California in Los Angeles, CA, USA. Since his Ph.D., Dr. Brooker was Professor of Pharmacology at the University of Virginia, Professor and Chairman of Biochemistry and Molecular Biology at Georgetown University in Washington, D.C. and at Johns Hopkins University since 1998. He is currently the director of the Johns Hopkins University Microscopy Center in Rockville, MD USA. Dr. Brooker's research interests in molecular mechanisms of cardiac contraction, hormone desensitization and cancer cell resistance to chemotherapeutic agents led to his interests and developments in microscope optics. He also founded Atto Bioscience (now acquired by Becton-Dickinson & Co.) which developed and marketed a number of products such as the CARV white light spinning disk confocal microscope and the AttoArc variable intensity microscope arc light source in partnership with Carl Zeiss. His current interests are in developing non-scanning holography and widefield 2-photon microscopy for fast and simple 3D fluorescence microscopy.

Guy Indebetouw is Professor Emeritus at Virginia Tech, USA. He obtained his Ph.D. in Applied Physics in 1976 at the Universitat Bern, Switzerland. His research interests include Holography, Imaging, Image Processing, Optical Metrology, Phase-conjugate Resonators, Optical Vortices, Photorefractive materials, and Liquid crystals. More recently, he pioneered the method of Scanning Holographic Microscopy, and expanded it to new grounds.

Natan T. Shaked received his B.Sc. and M.Sc. (Summa Cum Laude) degrees in electrical and computer engineering from Ben-Gurion University of the Negev, Beer Sheva, Israel, in 2002 and 2004, respectively, and has finished his Ph.D. studies in electrical and computer engineering at Ben-Gurion University of the Negev lately. His Ph.D. research interests include incoherent white-light holography and optical computing and processing. He has coauthor 13 refereed journal papers. Currently, he is a postdoctoral scholar in the Department of Biomedical Engineering, Duke University, North Carolina, USA.

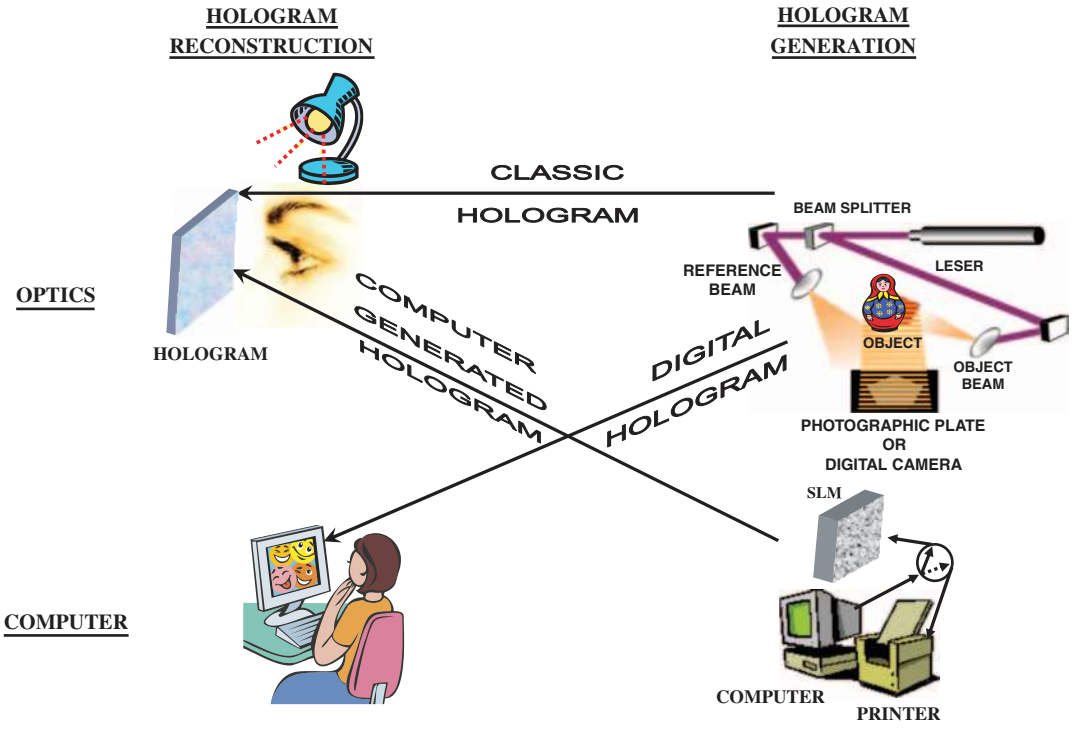

Fig. 1. Schematic of the mutual relations in holography discipline between digital computers and optics. SLM, spatial light modulator.

only two common aspects which exist in all these three methods. First, the system's input signal is always an incoherent light reflected or emitted from a certain 3-D scene. Second, the final product from all the three methods is a digital Fresnel hologram.

To understand the operation principle of any general Fresnel hologram, let us look on the difference between regular and Fresnel-holographic imaging systems. In classical imaging, image formation of objects at different distances from the lens results in a sharp image at the image plane for objects located at only one axial distance from the lens, as shown in Figure 2(a). The other objects located at different axial distances from the lens are out of focus. Fresnel holographic system, on the other hand, as depicted in Figure 2(b), projects a set of rings known as Fresnel zone plate (FZP) onto the plane of the image for each and every point at every plane of the 3-D object being viewed. The depth of the points is encoded by the density of the rings such that points which are closer to the system project less dense rings than distant points. Because of this encoding method, the 3-D information in the volume being imaged is recorded into the recording medium. Therefore, each plane in the image space reconstructed from a Fresnel hologram is in focus at a different axial distance. The encoding is accomplished by the presence of one of the holographic systems in the image path. Each holographic system, out of the three described herein, has a different method to project the FZP (or part of it) on the hologram plane. At this point it should be noted that this graphical description of projecting FZPs by every object's point actually expresses the mathematical 2-D correlation (or convolution) between the object function and the FZP. In other words, the three methods of creating incoherent Fresnel holograms are different from each other by the

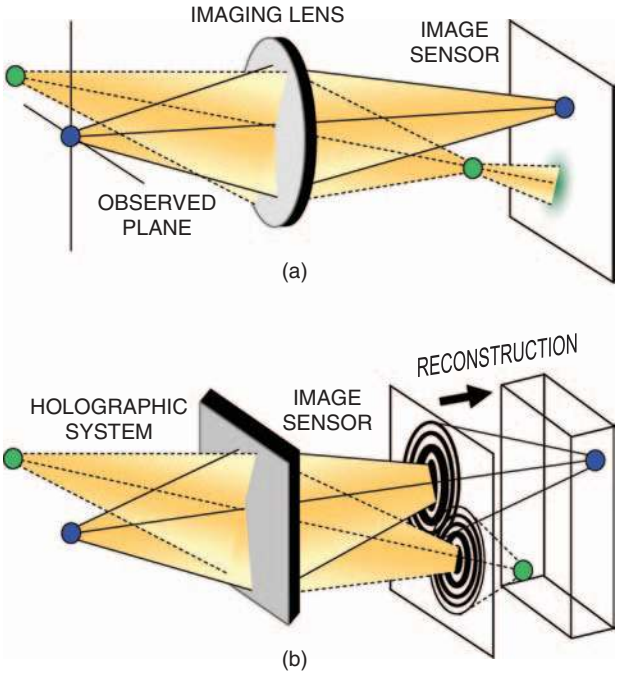

Fig. 2. Comparison of the Fresnel holography principle and conventional imaging. (a) Conventional imaging system. (b) Fresnel holography system.

way they spatially correlate the FZP with the 3-D scene. Another issue to note is that the correlation should be done with a FZP that is somehow 'sensitive' to the axial locations of the object points. Otherwise, these locations are not encoded into the hologram. All three systems described in this review satisfy differently the condition that the FZP is dependent on the axial distance of each and every object point. This means that indeed points, which are closer to the system, project FZP with fewer cycles per radial length than distant points, and by this condition the holograms can actually image the 3-D scene properly.

The FZP is a sum of at least three main functions, a constant bias, a quadratic phase function and its complex conjugate. The object function is actually correlated with all these three functions. However, the useful information, with which the holographic imaging is realized, is the correlation with just one of the two quadratic phase functions. The correlation with the other quadratic phase function induces the well-known twin image. Among the three methods of generating IDH, only the one described in Section 3 correlates the scene directly with a single quadratic phase function rather than with a complete FZP. This means that the detected signal in each of the other two holographic systems contains three superposed correlation functions, whereas only one of them is the required correlation between the object and the quadratic phase function. Therefore, the digital processing of the detected signal should have the ability to eliminate the two unnecessary terms.

The most mature technique among the three, and the only one that is extensively discussed in the literature, is the scanning holography, pioneered by Poon.[8–11] There are already a text book[10] and at least one review article[11] on scanning holography. Therefore, in the next section we only summarize shortly the fundamental principles of the classical scanning holography. However, we enlighten a more recent, and less known technique of the scanning holography, called homodyne scanning holography which our group has developed recently.[3]

A more-recently proposed digital hologram is the digital incoherent modified Fresnel hologram (DIMFH).[7] This hologram, described in Section 3, is actually a combination of computer-generated and digital holograms in the sense that although real existing objects are optically recorded, the process of the hologram generation is extensively computerized. Among the three methods this is the only one that does direct correlation of the scene with a quadratic phase function rather than with the complete FZP. Since the DIMFH is obtained as a direct correlation between the object and the quadratic phase function, the digital processing does not contain the procedure of removing the above-mentioned unnecessary correlation terms. Another unique feature of the hologram is its distinctive imaging scaling magnifications. Because of these unusual magnifications, this hologram is termed modified Fresnel hologram rather than just Fresnel hologram.

The third proposed IDH is dubbed Fresnel incoherent correlation hologram (FINCH).[4–6] The FINCH is actually based on a single channel incoherent correlator. Like the scanning holography, in the FINCH the object is correlated with a FZP, but the correlation is carried out without any movement and without multiplexing the image of the scene. Section 4 reviews the latest developments of the FINCH in the field of color holography and microscopy.

Following the description of the three methods in the next three sections, we compare between them and discuss their implementations in the last section.

2. SCANNING HOLOGRAPHY

Scanning holography[9–12] has demonstrated the ability to produce a Fresnel hologram of the incoherent light emission distributed in a 3-D structure. The definition of Fresnel hologram is any hologram that contains at least, a correlation (or convolution) between an object function and a quadratic phase function. Moreover, the quadratic phase function must be parameterized according to the axial distance of the object points from the detection plane. In other words, the number of cycles per radial distance of each quadratic phase function in the correlation is dependent on the axial distance of each object point. Formally, a hologram is called Fresnel hologram if it contains the following term:

$$H(u,v)=\iiint g(x,y,z) \times \exp\left[i\frac{2\pi\gamma}{z}[(u-x)^2+(v-y)^2]\right]dx\,dy\,dz \quad (1)$$

where $g(x, y, z)$ is the 3-D object function and γ is a constant. Indeed, in Eq. (1) the phase of the exponent is dependent on z, the axial location of the object. In case the object is illuminated by coherent wave, $H(u, v)$ given by Eq. (1) is the complex amplitude of the electromagnetic field directly obtained, under the paraxial approximation,[13] by free propagation from the object to the detection plane. However, we deal here with incoherent illumination, for which alternative methods to the free propagation should be applied. In fact, in this review we describe three different methods to get the desired correlation with the quadratic phase function given in Eq. (1), and all the three methods operate under incoherent illumination. Scanning holography is one of these methods to be described next.

In scanning holography the required correlation is performed by a mechanical movement. More specifically, a certain pattern, which is the above mentioned FZP, is projected on the observed object, whereas the FZP moves at a constant velocity relative to the object (or the object moves relative to the FZP). During the movement, the product between the FZP and the object is summed by a detector in discrete times. In other words, the pattern of the FZP scans the object and at each and every scanning

position the light intensity is integrated by the detector. The resulting electric signal is a sampled version of the 2-D correlation between the object and the FZP. The dependence of the FZP in the axial position of object points is achieved by interfering two mutually coherent, monochromatic, spherical waves on the object surface. The number of cycles per radial distance in each of the spherical waves is dependent on their axial interference location. Since these beams interfere on the object, the axial distance of each object point is stored in the hologram due to the fact that each point is correlated with a FZP the cycle density of which is dependent on the point's 3-D location.

Classic scanning holograms[9–11] have been recorded by a heterodyne interferometer in which the holographic information has been encoded on a high carrier frequency. Such method suffers from several drawbacks. On one hand, trying to keep the scanning time as short as possible requires using carrier frequencies which may be higher than the bandwidth limit of some, or all of the electronic devices in the system. On the other hand, working with a carrier frequency that is lower than the system limitation extends the scanning time far beyond the minimal time needed to capture the holographic information according to the sampling theorem. Long scanning times limit the system from recording dynamical scenes.

In the scanning holography described in Ref. [3], the required correlation is performed by scanning the object with a set of frozen-in-time FZP patterns. In this modified system, the hologram is recorded without temporal carrier frequency, using a homodyne interferometer. This offers an improved method of 3-D imaging which can be applied to incoherent imaging in general and to fluorescence microscopy in particular. The FZP is created by interference of two mutually-coherent spherical waves. As shown in Figure 3, the interference pattern is projected on the specimen, scans it in 2-D, and the reflected light from the specimen is integrated on a detector. Due to the line-by-line scanning by the FZP along the specimen, the one dimensional detected signal is composed of the entire lines of the correlation matrix between the object function and the FZP. In the computer, the detected signal is reorganized in the shape of a 2-D matrix, the values of which actually represent the Fresnel hologram of the specimen. The specimen we consider is 3-D, and its 3-D structure is stored in the hologram by the effect that during the correlation, the number of cycles per radial distance of the FZP, contributed from a distant object point, is slightly smaller than the number of cycles per radial distance of the FZP, contributed from a closer object point.

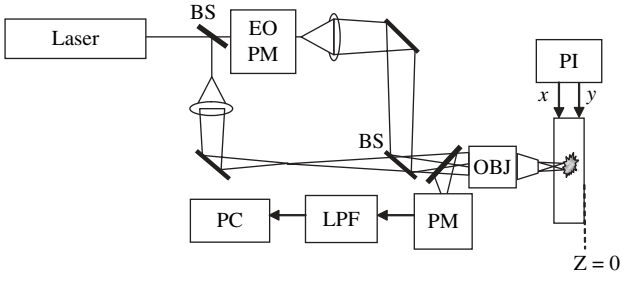

Fig. 3. Optical setup of the homodyne scanning holography system: EOPM, electro-optic phase modulator introducing a phase difference between the two beams; BS, beam splitter; PI, piezo XY stage, OBJ, objective; PM, photomultiplier tube detector; LPF, lowpass filter; PC, personal computer.

As mentioned above, the FZP is the intensity pattern of the interference between two spherical waves given by,

$$F(x,y,z) = Ap(x,y)\left\{2+\exp\left[\frac{i\pi}{\lambda(z_o+z)}(x^2+y^2)+i\theta\right]+\exp\left[\frac{-i\pi}{\lambda(z_o+z)}(x^2+y^2)-i\theta\right]\right\} \quad (2)$$

where $p(x, y)$ is a disk function with the diameter D that indicates the limiting aperture on the projected FZP, A is a constant, θ is the phase difference between the two spherical waves and λ is the wavelength of the coherent light source. The constant z_o indicates that at a plane $z = 0$, there is effectively interference between two spherical waves, one emerging from a point at $z = -z_o$ and the other converging to a point at $z = z_o$. This does not necessarily imply that these particular spherical waves are exclusively needed to create the FZP. For a 3-D object $S(x, y, z)$, the correlation with the FZP of Eq. (2) is,

$$\begin{aligned} H(x,y) &= \int S(x,y,z') * F(x,y,z')\,dz' \\ &= \int S(x',y',z')p(x'-x,y'-y)\,dz' \\ &\quad + \iiint S(x',y',z')p(x'-x,y'-y) \\ &\quad \times \exp\left\{\frac{i\pi[(x'-x)^2+(y'-y)^2]}{\lambda(z_o+z')}+i\theta\right\}dx'\,dy'\,dz' \\ &\quad + \iiint S(x',y',z')p(x'-x,y'-y) \\ &\quad \times \exp\left\{\frac{-i\pi[(x'-x)^2+(y'-y)^2]}{\lambda(z_o+z')}-i\theta\right\}dx'\,dy'\,dz' \end{aligned} \quad (3)$$

where the asterisk denotes a 2-D correlation. This correlation result is similar to a conventional Fresnel on-axis digital hologram,[14] and therefore, it suffers from the same problems. Specifically, $H(x, y)$ of Eq. (3) contains three terms which represent the information on three images namely the 0th diffraction order, the virtual, and the real images. Trying to reconstruct the image of the object directly from a hologram of the form of Eq. (3) would fail because of the disruption originated from two images out of the three. This difficulty is solved here with the same solution applied in a conventional on-axis digital holography. Explicitly, at least three holograms of the same specimen are recoded, where for each one of them a FZP with a

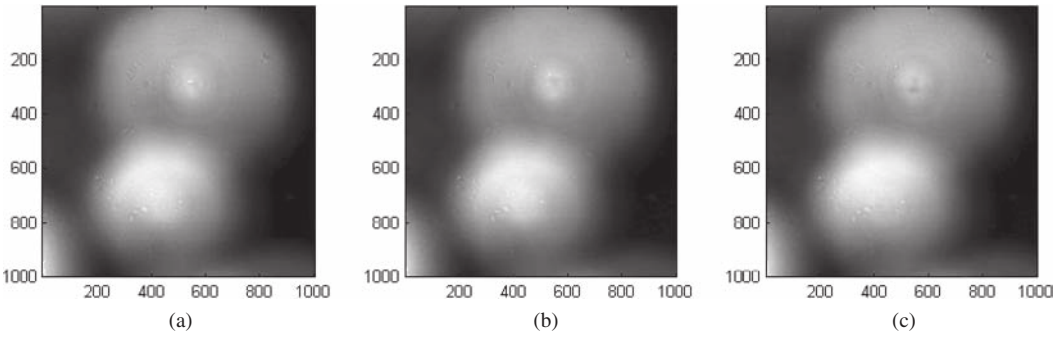

Fig. 4. Three recorded holograms with phase difference between the two interferometers arms of (a) 0, (b) $\pi/2$, and (c) π, all obtained from the homodyne scanning holography system.

different phase value θ is introduced. A linear combination of the three holograms cancels the two undesired terms and the remaining is a complex valued on-axis Fresnel hologram which contains only the information of the single desired image, either the virtual or the real one, according to our choice. A possible linear combination of the three holograms to extract a single correlation between the object and one of the quadratic phase functions of Eq. (3), is

$$\begin{aligned} H_{\mathrm{F}}(x,y) = {} & H_1(x,y)[\exp(\pm i\theta_3) - \exp(\pm i\theta_2)] \\ & + H_2(x,y)[\exp(\pm i\theta_1) - \exp(\pm i\theta_3)] \\ & + H_3(x,y)[\exp(\pm i\theta_2) - \exp(\pm i\theta_1)] \end{aligned} \quad (4)$$

where $H_i(x,y)$ is the i-th recorded hologram of the form of Eq. (3), and θ_i is the phase value of the i-th FZP used during the recording process. The choice between the signs in the exponents of Eq. (4) determines which image, virtual or real, is kept in the final hologram. If for instance the real image is kept, $H_{\mathrm{F}}(x,y)$ is the final complex-valued hologram of the form,

$$H_{\mathrm{F}}(x,y) = \int s(x,y,z') * p(x,y) \times \exp\left[\frac{-i\pi}{\lambda(z_{\mathrm{o}}+z')}(x^2+y^2)\right] dz' \quad (5)$$

The function $H_{\mathrm{F}}(x,y)$ is the final hologram which contains the information of only one image—the 3-D virtual image of the specimen in this case. Such image $S'(x,y,z)$ can be reconstructed from $H_{\mathrm{F}}(x,y)$ by calculating in the computer the inverse operation to Eq. (5), as follows,

$$S'(x,y,z) = H_{\mathrm{F}}(x,y) * \exp\left[\frac{i\pi}{\lambda z}(x^2+y^2)\right] \quad (6)$$

The resolution properties of this imaging technique are determined by the properties of the FZP. More specifically, the diameter D and the constant z_{o} characterize the system resolution in a similar way to the effect of an imaging lens.[13] Suppose the image is a single infinitesimal point at $z = 0$, then $H_{\mathrm{F}}(x,y)$ gets the shape of a quadratic phase function limited by a finite aperture. The reconstructed point image has a transverse diameter of $1.22\ \lambda z_{\mathrm{o}}/D$, which defines the transverse resolution, and an axial length of $8\ \lambda z_{\mathrm{o}}^2/D^2$, which defines the axial resolution. Note also

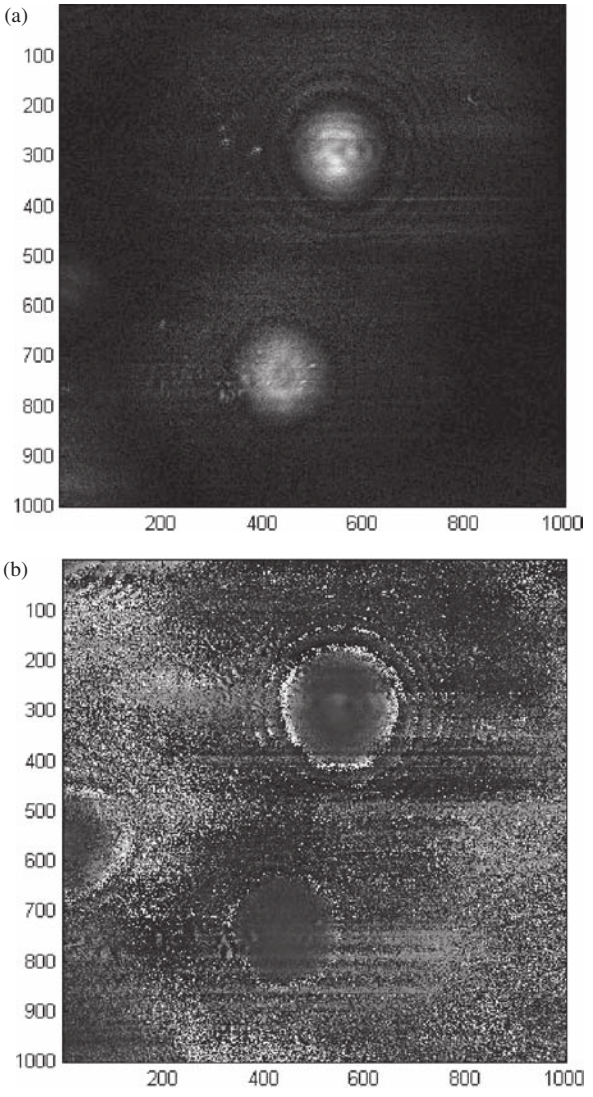

Fig. 5. (a) The magnitude and (b) the phase of the final homodyne scanning hologram.

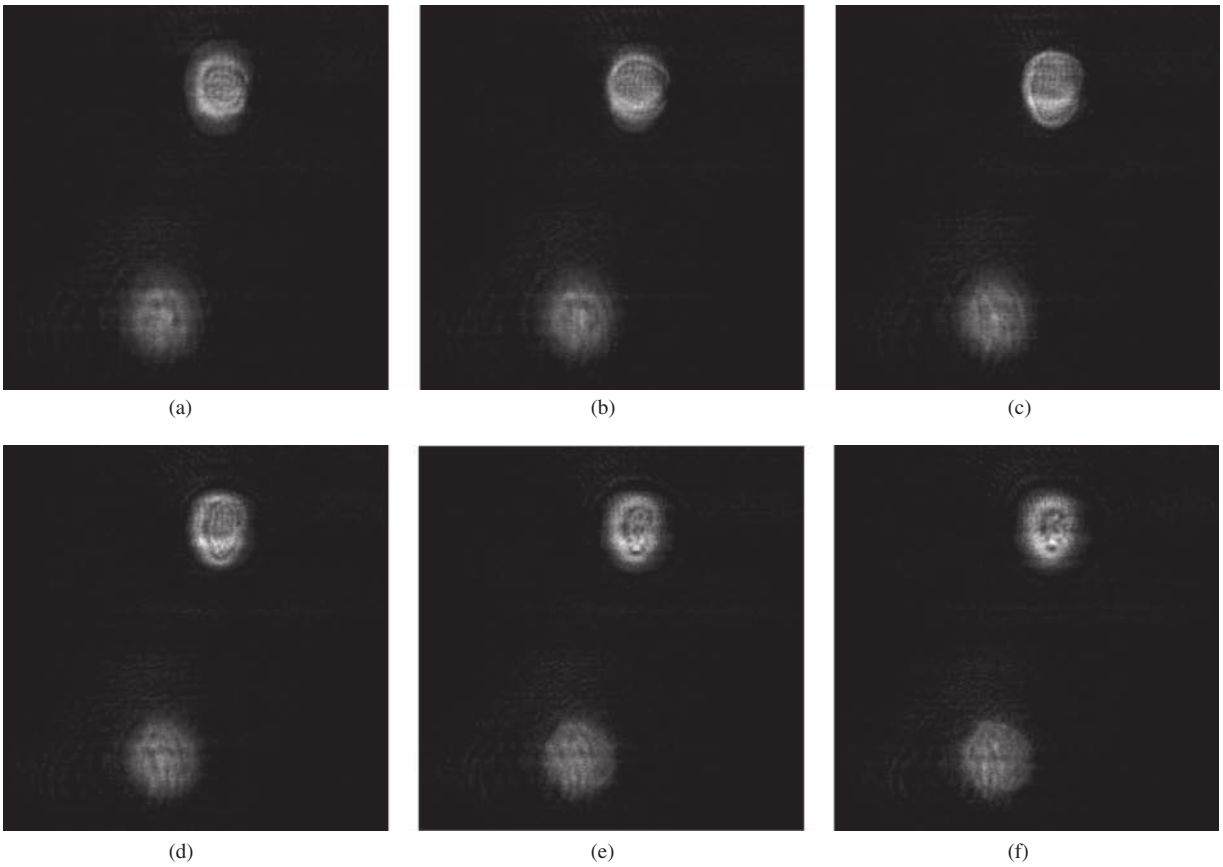

Fig. 6. (a–f) Various digital reconstructed images along the light propagation axis obtained by digital reconstruction from the hologram of Figure 5.

that the width of the FZP's last ring along its perimeter is about $\lambda z_o/D$, and therefore the size of the specimen's smallest distinguishable detail is approximately equal to the width of this ring.

As an example of the homodyne scanning hologram, let us describe the experiment from Ref. [3]. The setup shown in Figure 3 was built on a standard wide-field fluorescence microscope. The specimen was a slide with two pollen grains positioned at different distances from the microscope objective (infinity corrected $20\times$, NA $= 0.75$). The slide was illuminated by the FZP created by the interferometer. A laser beam ($\lambda = 532$ nm) was split in two beams with beam expanders consisting each of a microscope objective and a 12 cm focal-length achromat as a collimating lens. One of the beams passed through an electro-optic phase modulator driven by three (or more) constant voltage values, which induce three (or more) phase difference values between the interfering beams. Note that unlike previous studies,[9–12] there is no frequency difference between the two interfering waves since this time we record a hologram with a homodyne interferometer. The two waves were combined by the beam splitter to create an interference pattern in the space of the specimen. The pattern was then reduced in size and projected through the objective onto the specimen. The sample was scanned in a 2-D raster with an X–Y piezo stage. The data were collected by an acquisition system, and data manipulation was performed by the MATLAB software.

The three recorded holograms of the specimen taken with phase difference values of $\theta_{1,2,3} = 0,\ \pi/2$, and π are shown in Figures 4(a, b, and c), respectively. In this figures, the dominant term is the low frequency term [the first in Eq. (3)], and therefore, without mixing the three holograms in the linear combination that eliminates the low frequency along with the twin image term, there is no possibility to recover the desired image with a reasonable quality. These three holograms are substituted into Eq. (4) and yield a complex valued hologram shown in Figure 5. This time the grating lines are clearly revealed in the phase pattern. The computer reconstruction of two pollen grains along the z axis is shown in Figure 6. As can be seen in this figure, different parts of the pollen grains are in focus at different transverse planes.

3. DIGITAL INCOHERENT MODIFIED FRESNEL HOLOGRAPHY (DIMFH)

In this section, we review a recently-proposed method of holographic computer-aided imaging termed digital incoherent modified Fresnel holography (DIMFH).[7, 15–17]

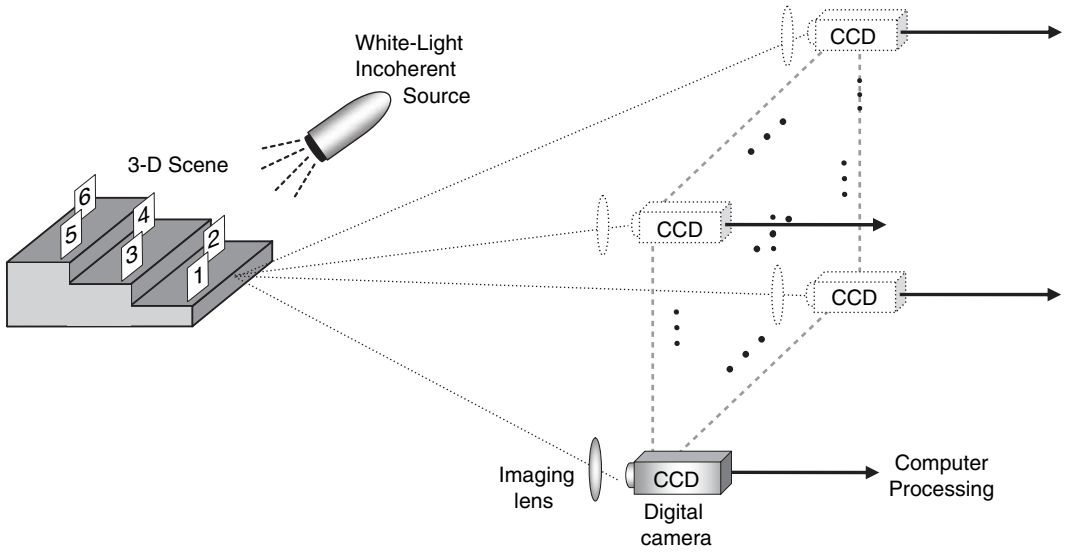

Fig. 7. Optical system for capturing multiple-viewpoint projections of the 3-D scene for obtaining a two-dimensional DIMFH of the scene. The camera and its imaging lens move together into a different capturing viewpoint for each projection.

Unlike the other two methods in this article, the DIMFH formation is not involved with interference between light beams of any kind. Generally in this method, a hologram is computed from a set of angular perspective projections of the observed 3-D object. Multiple-viewpoint projection holograms were first proposed by Li et al.[18] and further developed by Abookasis and Rosen,[19,20] and Sando et al.[21] These projections are captured by a conventional digital camera and numerically processed to yield a two-dimensional complex function, which is actually the desired digital Fresnel hologram. It is important to note that this hologram is not related to the well-known composite or stereoscopic holograms.[22] Unlike the composite hologram, the DIMFH is equivalent to an optical coherent hologram of the same scene recorded from the central point of view. In the DIMFH, although objects in the scene are captured by a conventional digital camera without wave interference, the process yields a hologram of the observed 3-D scene.

One disadvantage of the DIMFH is the complication of acquiring the large number of viewpoint projections of the 3-D scene needed to generate a high-resolution hologram. Therefore, we have recently proposed two different methods to make the projection acquisition more efficient. In the first method, we use a microlens array for acquiring the entire viewpoint projections of the 3-D scene in a single camera shot.[23] In the second method, we acquire only a small number of extreme projections and predict the middle projections in the computer by use of the view synthesis algorithm.[24] Using a macrolens array and the view synthesis algorithm[17] enables the DIMFH generation of moving 3-D objects with higher resolution than that of DIMFH implemented with a microlens array.

Figure 7 illustrates a possible optical system for acquiring multiple projections of the 3-D scene. In this case, the digital camera moves from one location to another, and each time acquires a single projection of the 3-D scene. Assuming that $2K+1$ projections of the 3-D scene are acquired on a 2-D grid, we number the projections by m and n, so that the middle projection is denoted by $(m,n)=(0,0)$, the upper-right projection by $(m,n)=(K,K)$ and the lower-left projection by $(m,n)=(-K,-K)$. Let $P_{m,n}(x_\mathrm{p},y_\mathrm{p})$ be the (m,n)th projection, where x_p and y_p are the axes on the projection plane. According to the proposed method, the (m,n)th projection $P_{m,n}(x_\mathrm{p},y_\mathrm{p})$ is multiplied by a quadratic phase function and the result is summed to the (m,n)th pixel in the final matrix as follows:

$$H(m,n)=\iint P_{m,n}(x_\mathrm{p},y_\mathrm{p}) \times \exp[i2\pi b(x_\mathrm{p}^2+y_\mathrm{p}^2)]\,dx_\mathrm{p}\,dy_\mathrm{p} \quad (7)$$

where b is an adjustable parameter. The process described by Eq. (7) is repeated for all the projections, so that each projection contributes a different pixel to the final matrix $H(m,n)$.

We now show that the 2-D complex matrix $H(m,n)$, obtained from the multiple projections according to Eq. (7), indeed represents the modified Fresnel hologram of the observed 3-D scene. Let us define the relation between an arbitrary point on the 3-D object and its projected point on the (m,n)th projection plane $P_{m,n}(x_\mathrm{p},y_\mathrm{p})$. Figure 8 illustrates a top view of the optical system shown in Figure 7. By using simple geometric relationships for the quantities illustrated in Figure 8, the coordinates of the projection plane are

$$x_\mathrm{p}=\frac{f(x_\mathrm{s}-m\alpha)}{z_\mathrm{s}}; \qquad y_\mathrm{p}=\frac{f(y_\mathrm{s}-n\alpha)}{z_\mathrm{s}} \quad (8)$$

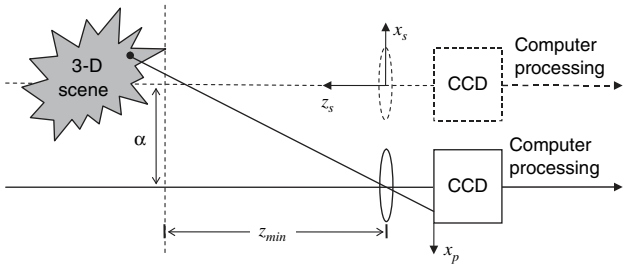

Fig. 8. Top view of the optical system shown in Figure 7.

where x_s, y_s and z_s are the axes of the 3-D scene, f is the focal length of the imaging lens, and α is the camera (and the imaging lens) gap between two adjacent projections. Let us look at a single object point, with an infinitesimal size of $(\Delta x_s, \Delta y_s, \Delta z_s)$ located on the 3-D scene at coordinates (x_s, y_s, z_s) and having a value of $h(x_s, y_s, z_s)$. Using Eqs. (7) and (8), the complex amplitude distribution obtained on the hologram plane by this source point is

$$\begin{aligned}\tilde{H}(m,n;x_s,y_s,z_s)&=\iint[h(x_s,y_s,z_s)\Delta x_s\Delta y_s\Delta z_s\delta(x'_p-x_p,y'_p-y_p)]\\&\quad\times\exp[i2\pi b(x'^2_p+y'^2_p)]\,dx'_p\,dy'_p\\&=h(x_s,y_s,z_s)\exp[i2\pi b(x_p^2+y_p^2)]\Delta x_s\Delta y_s\Delta z_s\\&=h(x_s,y_s,z_s)\exp\left[\frac{i2\pi bf^2}{z_s^2}[(x_s-m\alpha)^2\right.\\&\quad\left.+(y_s-n\alpha)^2]\right]\Delta x_s\Delta y_s\Delta z_s\end{aligned}\tag{9}$$

where δ is the Dirac delta function. The overall complex amplitude distribution of the hologram resulting from all the 3-D scene points is a volume integral over all the coinciding holograms of the individual source points, as follows:

$$\begin{aligned}H(m,n)&=\iiint\tilde{H}(m,n;x_s,y_s,z_s)\,dx_s\,dy_s\,dz_s,\\&=\iiint h(x_s,y_s,z_s)\\&\quad\times\exp\left[i2\pi bf^2\frac{(x_s-m\alpha)^2+(y_s-n\alpha)^2}{z_s^2}\right]dx_s\,dy_s\,dz_s\end{aligned}\tag{10}$$

Equation (10) has the similar functional behavior of a digital Fresnel hologram of the 3-D scene as is expressed by Eq. (1). However, in spite of this similarity, there are still several differences between a conventional imaging system and the proposed hologram. These differences are described next.

To get the reconstructed plane $s(m, n; z_r)$, located at axial distance z_r from the hologram $H(m, n)$, this hologram is digitally correlated with a quadratic phase function as follows:

$$s(m,n;z_r)=\left|H(m,n)*\exp\left[-\frac{i2\pi}{\zeta z_r}((m\Delta p)^2+(n\Delta p)^2)\right]\right|\tag{11}$$

where Δp is the pixel size of the digital camera and ζ is an adjustable parameter. From Eqs. (10) and (11), one can see that the axial positions of the objects reconstructed from the hologram are proportional to the square of the coinciding axial positions of the original objects. To obtain the transverse magnifications M_x and M_y of the proposed hologram, we first rewrite Eq. (10) as follows:

$$\begin{aligned}H(m,n)&=\iiint h(x_s,y_s,z_s)\exp\left[i2\pi b\left(\frac{M\alpha}{\Delta p}\right)^2\left[\left(\frac{\Delta px_s}{\alpha}-m\Delta p\right)^2\right.\right.\\&\quad\left.\left.+\left(\frac{\Delta py_s}{\alpha}-n\Delta p\right)^2\right]\right]dx_s\,dy_s\,dz_s\end{aligned}\tag{12}$$

where $M = f/z_s$ is the magnification of the imaging lens. Equation (12) shows that the hologram is actually a sampling pattern of the scene by a 2-D sampling function, which creates unique transverse magnifications. The quadratic phase function magnifies the object's size by the constant $\Delta p/\alpha$. We conclude that the resulting transverse magnifications M_x and M_y of the proposed hologram are $M_x = M_y = \Delta p/\alpha$. This indicates that, contrary to a conventional imaging system, the magnification of the DIMFH is constant and is independent of the axial positions of the objects in the 3-D scene. This effect can be eliminated by rescaling the reconstructed planes along the two transverse axes by M/M_x. On the other hand, we have also shown that this effect can be useful for optical 3-D object recognition, since only one matched filter can be

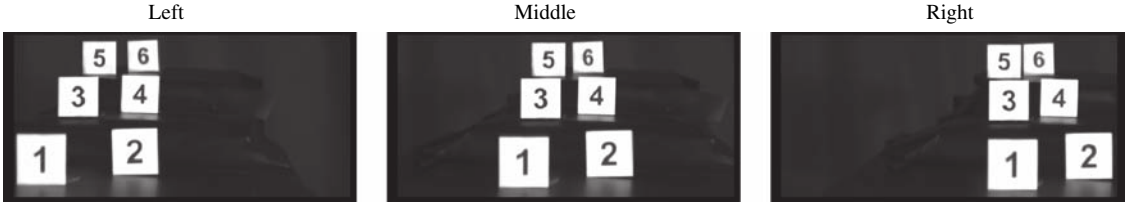

Fig. 9. (a–c) Three projections taken from the entire projection set obtained by the system shown in Figure 7, but with horizontal movement only of the camera.

used to detect all identical objects in the 3-D scene, no matter how close to or far from the acquisition plane these objects are.[16]

As an example of the DIMFH, we describe the experiment firstly presented in Ref. [7]. To simplify the experimental setup there, the multiple projections were captured along the horizontal axis only (in contrast to the optical system shown in Fig. 7). By doing this, only a 1D DIMFH was generated by the optical system. Six planes, each 2.5 cm × 2.5 cm, containing the digits 1–6, were positioned on a dark background and used as the 3-D scene. The distances between the plane containing the digit 1 and the planes containing the digits 2, 3, 4, 5, and 6 were 4, 0, 4, 0, and 4 cm on the horizontal x_s axis; 0, 3.5, 3.5, 6.5, and 6.5 cm on the vertical y_s axis; and 5, 12, 17, 23.5, and 28.5 cm on the optical z_s axis, respectively. The distance between the closest plane containing the digit 1 and the imaging lens was 43 cm. The camera used was a CCD camera containing 1280 × 1024 pixels and an 8.6 mm × 6.9 mm active area. Figures 9(a–c) show 3 projections out of the 500 projections acquired by the camera across a horizontal range of 10 cm. As shown in this figure, the relative positions of the digits change only along the horizontal axis (but not along the vertical axis) as a

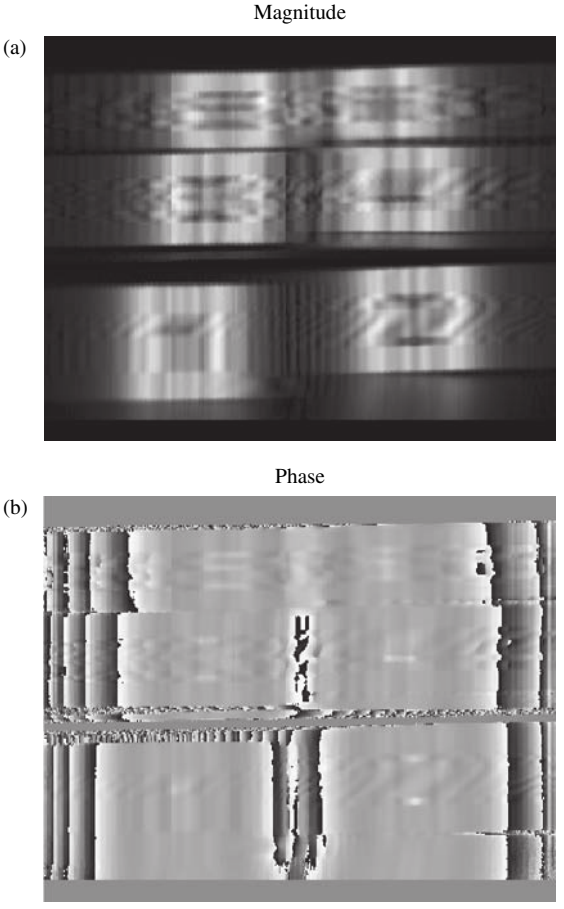

Fig. 10. (a) Magnitude and (b) phase of the one-dimensional DIMFH.

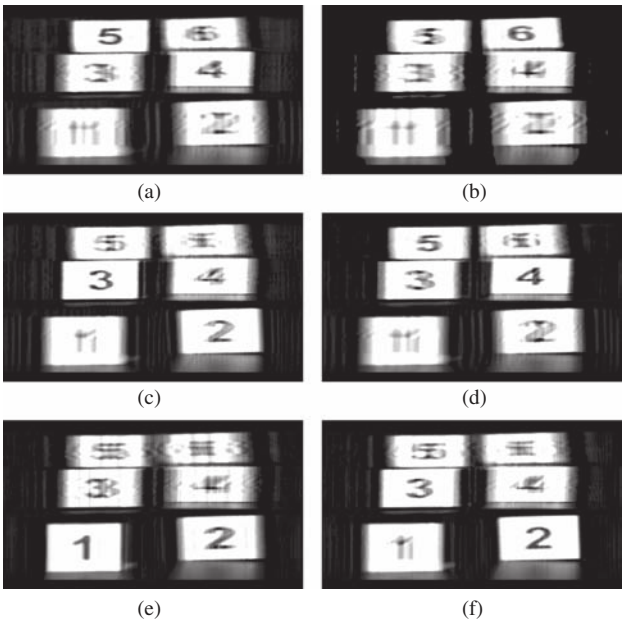

Fig. 11. (a–f) The six best in-focus reconstructed planes along the optical axis obtained by digital reconstruction from the hologram of Figure 10.

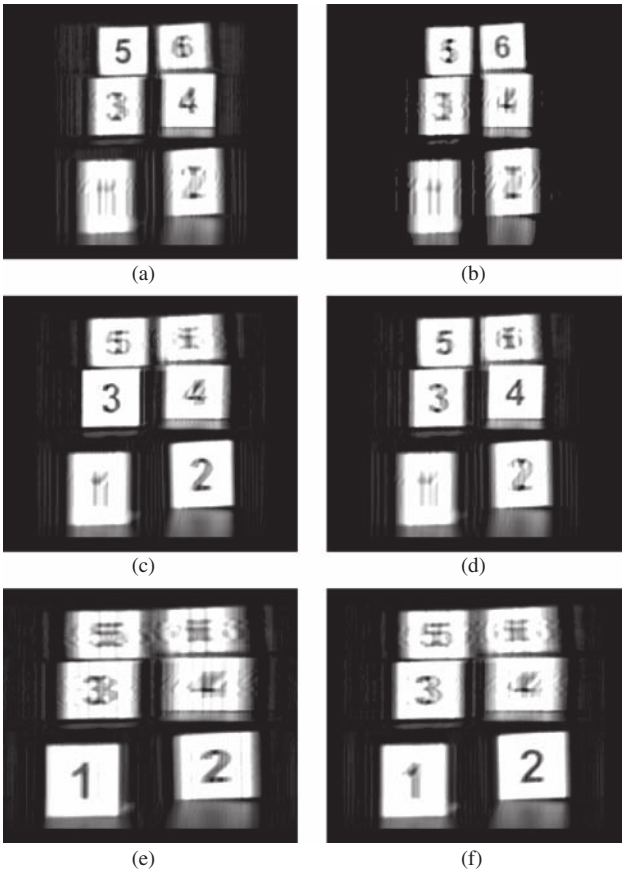

Fig. 12. (a–f) The six best in-focus reconstructed planes along the optical axis, obtained by digital reconstruction from the hologram of Figure 10, after the rescaling process of the horizontal axis.

function of the location of the projection in the entire set of projections. Each of the acquired projections was multiplied, according to Eq. (7) by a 1-D quadratic phase function, and the result was summed to a single column in the 1-D DIMFH of the 3-D scene. Figures 10(a) and (b) show the magnitude and the phase of the hologram obtained from this procedure, respectively. Digital reconstruction of the 3-D scene recorded into the DIMFH was obtained by correlating the hologram with a 1-D quadratic phase function. Figures 11(a–f) show six chosen planes reconstructed along the optical axis. In each plane, a different digit is in focus, whereas the other five digits are out of focus. This behavior validates the volumetric information encoded into the hologram. As explained above, rescaling these reconstructed planes along the horizontal axis by a factor of M/M_x is required to retain the original aspect ratios of the objects. Figures 12(a–f) show the best in-focus reconstructed planes, rescaled on the horizontal axis by M/M_x. Following the rescaling process, the aspect ratios of the reconstructed objects in each of the best in-focus planes are indeed identical to the aspect ratios of the objects in the original 3-D scene.

4. FRESNEL INCOHERENT CORRELATION HOLOGRAPHY

In this section we review the FINCH—the third method of recording digital Fresnel holograms under incoherent illumination. Various aspects of the FINCH have been described in Refs. [4–6], including FINCH of reflected white light,[4] FINCH of fluorescence objects[5] and finally FINCHSCOPE[6]—a holographic fluorescence microscope. We briefly review these works in the current section.

Generally, in the FINCH system the reflected white light from a 3-D object propagates through a diffractive optical element (DOE) and is recorded by a digital camera. To solve the twin image problem, three holograms are recorded sequentially, each with a different phase factor of the DOE. The three holograms are superposed in the computer such that the result is a complex-valued Fresnel hologram. The 3-D properties of the object are revealed by reconstructing this hologram in the computer.

One of the FINCH systems[4] is shown in Figure 13. A white-light source illuminates a 3-D object, and the reflected light from the object is captured by a CCD camera after passing through a lens L and a DOE displayed on a spatial light modulator (SLM). In general, such a system can be analyzed as an incoherent correlator, where the DOE function is considered as a part of the system's transfer function. However, in this review, we find it easier to regard the system as an incoherent interferometer, where the grating displayed on the SLM is considered as a beam splitter. As is common in such cases, we analyze the system by following its response to an input object of a single infinitesimal point. Knowing the system's point

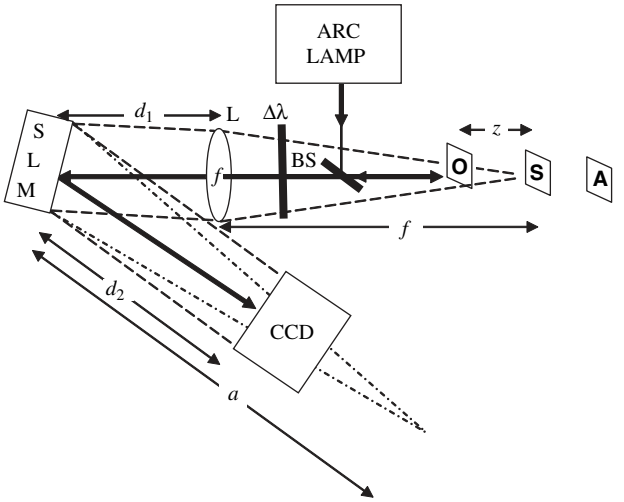

Fig. 13. Schematic of FINCH recorder. BS: beam splitters; SLM: spatial light modulator; CCD: charge-coupled device; L is a spherical lens with $f = 25$ cm focal length. $\Delta\lambda$ indicates a chromatic filter with a bandwidth of $\Delta\lambda = 60$ nm.

spread function (PSF) enables one to realize the system operation for any general object. Analysis of a beam originated from a narrowband infinitesimal point source is done using Fresnel diffraction theory,[13] since such a source is coherent by definition.

A Fresnel hologram of a point object is obtained when the two interfering beams are, for instance, plane and spherical beams. Such a goal is achieved if the DOE's reflection function $R(x_D, y_D)$ is of the form

$$R(x_D, y_D) = \frac{1}{2} + \frac{1}{2}\exp\left[-\frac{i\pi}{\lambda a}(x_D^2 + y_D^2) + i\theta\right] = \frac{1}{2} + \frac{1}{2}Q\left(-\frac{1}{a}\right)\exp(i\theta) \quad (13)$$

For the sake of shortening, the quadratic phase function is designated by the function Q, such that $Q(b) = \exp[i\pi b/\lambda(x^2 + y^2)]$. The first constant term 1/2 in Eq. (13) represents the plane wave, and the quadratic phase term is responsible for the spherical wave. The angle θ plays an important role later in the computation process to get rid of the twin image and the bias term, in the same way it is done in the case of the homodyne scanning hologram described in Section 2.

A point source located at the point $(0, 0, z_s)$ a distance $f - z_s$ from a spherical positive lens, with f focal length, induces on the lens plane a diverging spherical wave of the form of $Q(1/f - z_s)$. Right after the lens, which has a transmission function of $Q(-1/f)$, the complex amplitude of the wave is $Q(1/f - z_s)Q(-1/f) = Q[z_s/f(f - z_s)]$. After propagating additional distance of d_1 till the DOE plane, the complex amplitude becomes $Q\{z_s/[f(f - z_s) + z_s d_1]\}$. Right after the DOE, with the reflection function given in Eq. (13),

the complex amplitude is related to $Q\{z_s/[f(f-z_s)+z_s d_1]\}[1+Q(-1/a)\exp(i\theta)]$. Finally, in the CCD plane at a distance d_2 from the DOE, the intensity of the recorded hologram is,

$$I_P(x,y) = A\left|Q\left[\left(\frac{f(f-z)}{z}+d_1+d_2\right)^{-1}\right] + Q\left[\left(\frac{af(f-z)+azd_1}{za-f(f-z)-zd_1}+d_2\right)^{-1}\right]\exp(i\theta)\right|^2 \quad (14)$$

where A is a constant. The first term of Eq. (14) is now approximated to a constant by assuming that z is much smaller than f. Since the system is shift invariant, the result of $I_P(x,y)$, after calculating the square magnitude in Eq. (14), can be generalized to a PSF for any source point located at any point (x_s, y_s, z_s), as follows,

$$I_P(x,y) = A\left(2+\exp\left\{\frac{i\pi}{\lambda\gamma(z)}\left[\left(x+\frac{ax_s}{f}\right)^2+\left(y+\frac{ay_s}{f}\right)^2\right]+i\theta\right\} + \exp\left\{\frac{-i\pi}{\lambda\gamma(z)}\left[\left(x+\frac{ax_s}{f}\right)^2+\left(y+\frac{ay_s}{f}\right)^2\right]-i\theta\right\}\right) \quad (15)$$

where, $\gamma(z) = [d_2 - a - z(d_1 a + d_2 f - af + d_2 a - d_1 d_2)f^{-2}]/[1-z(a+f-d_1)f^{-2}]$ For a general 3-D object $g(x_s, y_s, z_s)$ illuminated by a narrowband incoherent illumination, the intensity of the recorded hologram is an integral of the entire PSFs given in Eq. (15), over all object intensity $g(x_s, y_s, z_s)$, as follows

$$H(x,y) \cong A\left(C+\iiint g(x_s,y_s,z_s)\exp\left\{\frac{i\pi}{\lambda\gamma(z)}\left[\left(x+\frac{ax_s}{f}\right)^2+\left(y+\frac{ay_s}{f}\right)^2\right]+i\theta\right\}dx_s\,dy_s\,dz_s + \iiint g(x_s,y_s,z_s)\exp\left\{\frac{-i\pi}{\lambda\gamma(z)}\left[\left(x+\frac{ax_s}{f}\right)^2+\left(y+\frac{ay_s}{f}\right)^2\right]-i\theta\right\}dx_s\,dy_s\,dz_s \quad (16)$$

Besides a constant term C, Eq. (16) contains two terms of correlation between an object and a quadratic phase, z-dependent, function, which means that the recorded hologram is indeed a Fresnel hologram. In order to remain with a single correlation term out of the three terms given in Eq. (16), we again follow the usual procedure of on-axis digital holography.[14] Three holograms of the same object are recorded each of which with a different phase constant θ. The final hologram H_F is a superposition according to Eq. (4).

A 3-D image $s(x,y,z)$ can be reconstructed from $H_F(x,y)$ by calculating the Fresnel propagation formula, as follows,

$$s(x,y,z) = H_F(x,y) * \exp\left[\frac{i\pi}{\lambda z}(x^2+y^2)\right] \quad (17)$$

The system shown in Figure 13 was used to record the three holograms.[4] The SLM (Holoeye HEO 1080P) is phase-only, and as so, the desired function given by Eq. (13) cannot be directly displayed on this SLM. To overcome this obstacle, the phase function $Q(-1/a)$ is displayed on only half of the SLM pixels. The rest of the pixels were modulated with a constant phase, where the pixels of each kind were selected randomly. By this method the SLM function becomes a good approximation to $R(x_D, y_D)$ of Eq. (13).

The SLM has 1920×1080 pixels in a display of 16.6×10.2 mm, where only the central 1024×1024 pixels were used for implementing the DOE. The phase distribution of the three reflection masks displayed on the SLM, with phase constants of 0°, 120° and 240°, are shown in Figures 14(a, b, and c), respectively. The other specifications of the system are: $f = 250$ mm, $a = 430$ mm, $d_1 = 132$ mm, $d_2 = 260$ mm.

Three white on black letters each of the size 2×2 mm were located at the vicinity of rear focal point of the lens. 'O' was at $z = -24$ mm, 'S' was at $z = -48$ mm and 'A' was at $z = -72$ mm. These letters were illuminated by a mercury arc lamp. A filter which passed a Poisson-like power spectrum from 574 to 725 nm light with a peak wavelength of 599 nm and a bandwidth (full width at half maximum) of 60 nm was positioned between the beamsplitter and the lens L. The three holograms, each for a different phase constant of the DOE, were recorded by a CCD camera and processed by a PC. The final hologram $H_F(x,y)$ was calculated according to Eq. (4) and its magnitude and phase distributions are depicted in Figures 14(e) and (f), respectively.

The hologram $H_F(x,y)$ was reconstructed in the computer by calculating the Fresnel propagation toward various z propagation distances according to Eq. (17). Three different reconstruction planes are shown in Figures 14(g–i). In each plane, a different letter is in focus as is indeed expected from a holographic reconstruction of an object with a volume.

In Ref. [5] the FINCH has been capable to record multicolor digital holograms from objects emitting fluorescent light. The fluorescent light specific to the emission wavelength of various fluorescent dyes after excitation of 3-D objects was recorded on a digital monochrome camera after reflection from the DOE. For each wavelength of fluorescent emission, the camera sequentially records three holograms reflected from the DOE, each with a different phase factor of the DOE's function. The three holograms are again superposed in the computer to create

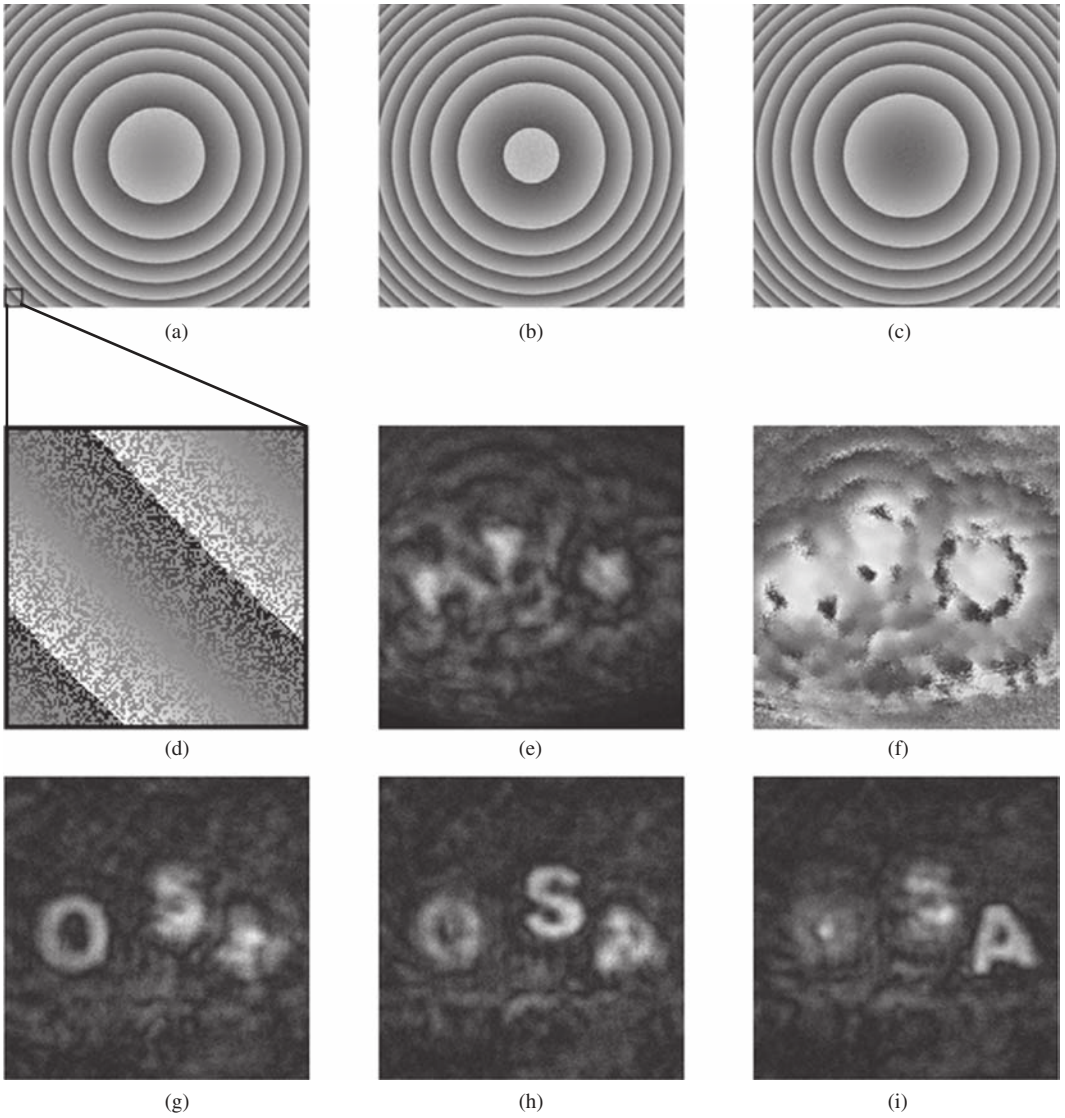

Fig. 14. FINCH results: (a) Phase distribution of the reflection masks displayed on the SLM, with $\theta = 0°$, (b) $\theta = 120°$, (c) $\theta = 240°$. (d) Enlarged portion of (a) indicating that half (randomly chosen) of the SLM's pixels modulate light with a constant phase. (e) Magnitude and (f) phase of the final on-axis digital hologram. (g) Reconstruction of the hologram of the three letters at the best focus distance of '*O*.' (h) Same reconstruction at the best focus distance of '*S*,' and (i) of '*A*.'

a complex-valued Fresnel hologram of each fluorescent emission without the twin image problem. The holograms for each fluorescent color are further combined in a computer to produce a multicolored fluorescence hologram and 3-D color image.

An experiment showing the recording of a color fluorescence hologram was carried out[5] on the system shown in Figure 15. The phase constants of $\theta_{1,2,3} = 0°$, 120°, 240° were introduced into the three quadratic phase functions. The other specifications of the system are: $f_1 =$ 250 mm, $f_2 = 150$ mm, $f_3 = 35$ mm, $d_1 = 135$ mm, $d_2 =$ 206 mm. The magnitude and phase of the final complex hologram, superposed from the first three holograms, are shown in Figures 16(a) and (b), respectively. The reconstruction from the final hologram was calculated using the Fresnel propagation formula of Eq. (17). The results are shown at the plane of the front face of the front die (Fig. 16(c)), and at the plane of the front face of the rear die (Fig. 16(d)). Note that in each plane a different die face is in focus as is indeed expected from a holographic reconstruction of an object with a volume. The second set of three holograms was recorded via a red filter in the emission filter slider F_2 which passed 614 to 640 nm fluorescent light wavelengths with a peak wavelength of 626 nm and a bandwidth of 11 nm (FWHM). The magnitude and phase of the final complex hologram, superposed from the 'red' set, is shown in Figures 16(e) and (f), respectively. The reconstruction results from this final hologram are shown in Figures 16(g) and (h) at the same planes as shown in Figures 16(c) and (d), respectively. Finally, an additional set of three holograms was recorded with a green filter in emission filter slider F_2, which passed 500 to

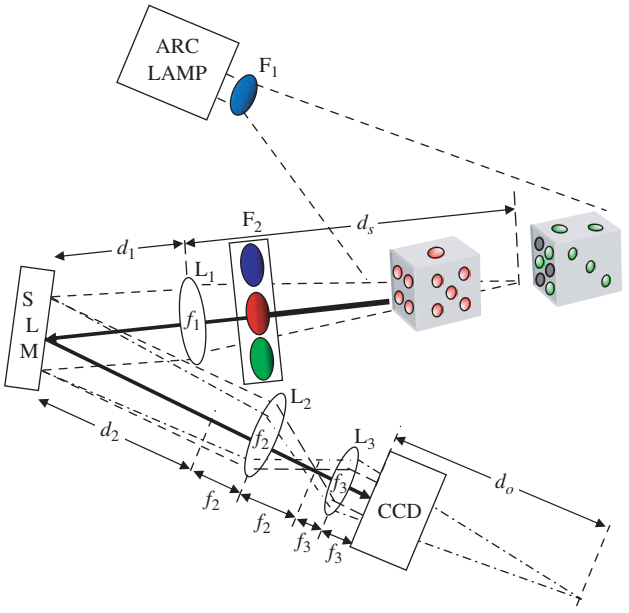

Fig. 15. Schematics of the FINCH color recorder. SLM: spatial light modulator; CCD: charge-coupled device; L_1, L_2, L_3 are spherical lenses and F_1, F_2 are chromatic filters.

532 nm fluorescent light wavelengths with a peak wavelength of 516 nm and a bandwidth of 16 nm (FWHM). The magnitude and phase of the final complex hologram, superposed from the 'green' set, is shown in Figures 16(i) and (j), respectively. The reconstruction results from this final hologram are shown in Figures 16(k) and (l) at the same planes as shown in Figures 16(c) and (d), respectively. Compositions of Figures 16(c), (g), and (k) and Figures 16(d), (h), and (l) are depicted in Figures 16(m) and (n), respectively. Note that all the colors in Figure 16 are pseudo-colors. These last results yield a complete color 3-D holographic image of the object including the red and green fluorescence. While the optical arrangement in this demonstration has not been optimized for maximum resolution, it is important to recognize that even with this simple optical arrangement, the resolution is good enough to image the fluorescent emissions with good fidelity and to obtain good reflected light images of the dice. Furthermore, in the reflected light images in Figures 16(c and m) the system has been able to detect a specular reflection of the illumination from the edge of the front dice.

The last system to be reviewed here is the first demonstration of a motionless microscopy system

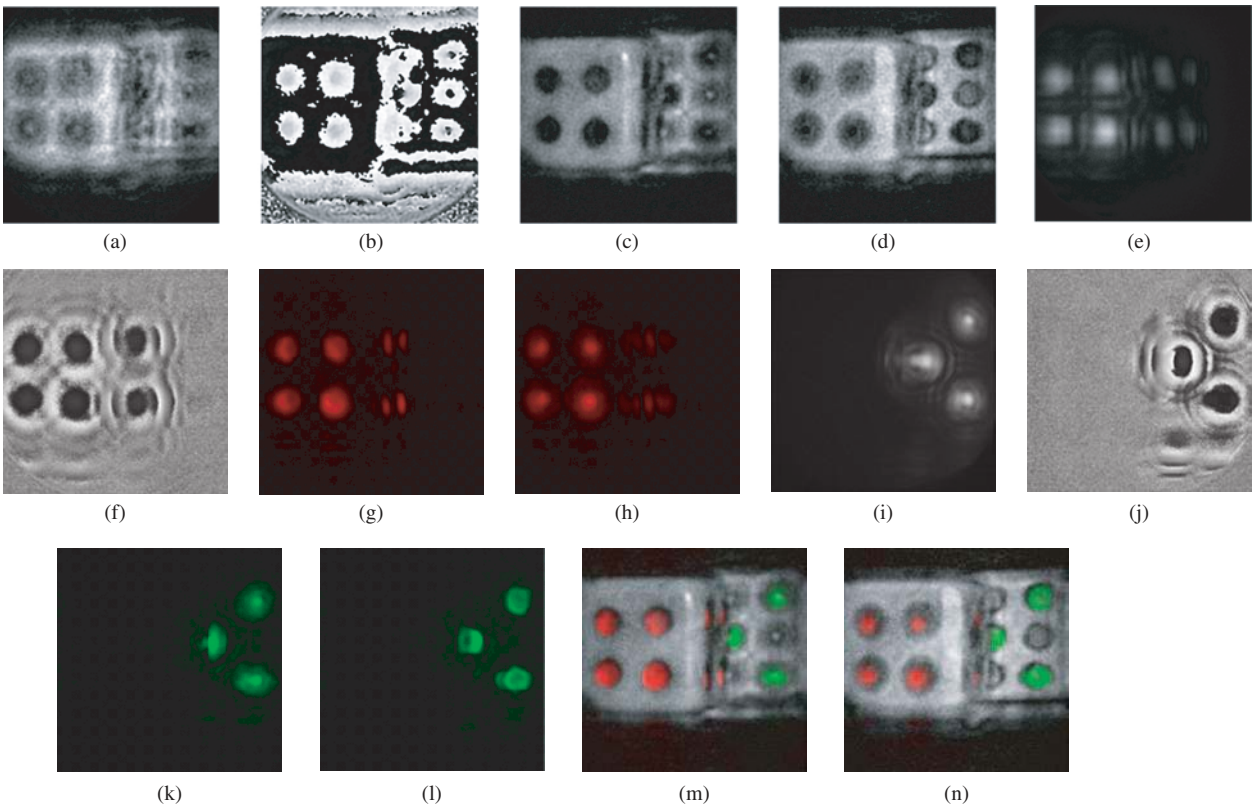

Fig. 16. (a) Magnitude and (b) phase of the complex Fresnel hologram of the dice. Digital reconstruction of the non-fluorescence hologram: (c) at the face of the red-dots on the die, and (d) at the face of the green dots on the die. (e) Magnitude and (f) phase of the complex Fresnel hologram of the red dots. Digital reconstruction of the red fluorescence hologram: (g) at the face of the red-dots on the die, and (h) at the face of the green dots on the die. (i) Magnitude and (j) phase of the complex Fresnel hologram of the green dots. Digital reconstruction of the green fluorescence hologram: (k) at the face of the red-dots on the die, and (l) at the face of the green dots on the die. Compositions of Figures 16(c), (g), and (k) and Figures 16(d), (h), and (l) are depicted in Figures 16(m) and (n), respectively.

(FINCHSCOPE) based upon the FINCH, and its use in recording high-resolution 3-D fluorescent images of biological specimens.[6] By using high-numerical-aperture lenses, a spatial light modulator, a charge-coupled device camera and some simple filters, FINCHSCOPE enables the acquisition of 3-D microscopic images without the need for scanning.

A schematic diagram of the FINCHSCOPE for an upright microscope equipped with an arc lamp source is shown in Figure 17. The beam of light that emerges from an infinity-corrected microscope objective transforms each point of the object being viewed into a plane wave, thus satisfying the first requirement of FINCH.[4] An SLM and a digital camera replace the tube lens, reflective mirror and other transfer optics normally present in microscopes. Because no tube lens is required, infinity-corrected objectives from any manufacturer can be used. A filter wheel was used to select excitation wavelengths from a mercury arc lamp, and the dichroic mirror holder and the emission filter in the microscope were used to direct light to and from the specimen through infinity-corrected objectives.

The ability of the FINCHSCOPE to resolve multicolour fluorescent samples was evaluated by first imaging polychromatic fluorescent beads. A fluorescence bead slide with the beads separated on two separate planes was constructed. FocalCheck polychromatic beads (6 μm) were used to coat one side of a glass microscope slide and a glass coverslip. These two surfaces were juxtaposed and held together at a distance from one another of $\sim$50 μm with optical cement. The beads were sequentially excited at 488, 555 and 640 nm center wavelengths (10–30 nm bandwidths)

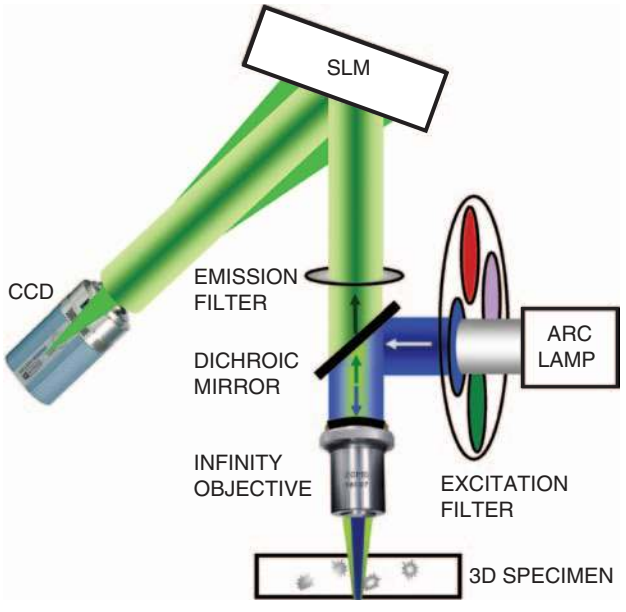

Fig. 17. FINCHSCOPE schematic in upright fluorescence microscope. The upright microscope was modified with a reflective SLM positioned at a tilt angle of 11° to reflect emission light from the objective onto the camera.

with emissions recorded at 515–535 nm, 585–615 nm and 660–720 nm, respectively. Figures 18(b–d) show reconstructed image planes from 6 μm beads excited at 640 nm and imaged on the FINCHSCOPE with a Zeiss PlanApo $\times$20, 0.75 NA objective. Figure 18(a) shows the magnitude of the complex hologram, which contains all the information about the location and intensity of each bead at every plane in the field. The Fresnel reconstruction from this hologram was selected to yield 49 planes of the image, 2 μm apart. Two beads are shown in Figure 18(b), with only the lower bead exactly in focus. The next image (Fig. 18(c)) is 2 μm into the field in the Z-direction, and the upper bead is now in focus, with the lower bead slightly out of focus. The focal difference is confirmed by the line profile drawn between the beads, showing an inversion of intensity for these two beads between the planes. There is another bead between these two beads, but it does not appear in Figures 18(b or c) (or in the intensity profile), because it is 48 μm from the upper bead; it instead appears in Figure 18(d) (and in the line profile), which is 24 sections away from the section in Figure 18(c). Notice that the beads in Figures 18(b and c) are no longer visible in Figure 18(d). In the complex hologram in Figure 18(a), the small circles encode the close beads and the larger circles encode the distant central bead. Figure 18(e) shows that the Z-resolution of the lower bead in Figure 18(b), reconstructed from sections created from a single hologram (blue line), is at least comparable to data from a widefield stack of 28 sections (obtained by moving the microscope objective in the Z-direction) of the same field (red line). The co-localization of the fluorescence emission was confirmed at all excitation wavelengths and at extreme Z limits as shown in Figures 18(f–m) for the 6 μm beads at the planes shown in Figures 18(b(f–i) and d(j–m)). In Figures 18(n–r), 0.5 μm beads (TetraSpeck, Invitrogen) imaged with a Zeiss PlanApo $\times$63 1.4 NA oil-immersion objective are shown. Figure 18(n) presents one of the holograms captured by the camera and Figure 18(o) shows the magnitude of the complex hologram. Figures 18(p–r) show different planes (6, 15 and 20 μm, respectively) in the bead specimen after reconstruction from the complex hologram of image slices in 0.5 μm steps. Arrows show the different beads visualized in different Z image planes. The computer reconstruction along the Z-axis of a group of fluorescently labeled pollen grains (Carolina Biological slide no. 30-4264) is shown in Figures 19(b–e). As is expected from a holographic reconstruction of a 3-D object with volume, any number of planes can be reconstructed. In this example, a different pollen grain was in focus in each transverse plane reconstructed from the complex hologram whose magnitude is shown in Figure 19(a). In Figures 19(b–e), the values of Z are 8, 13, 20 and 24 μm, respectively. A similar experiment was performed with the autofluorescent Convallaria rhizom and the results are shown in Figures 19(g–j) at planes 6, 8, 11 and 12 μm.

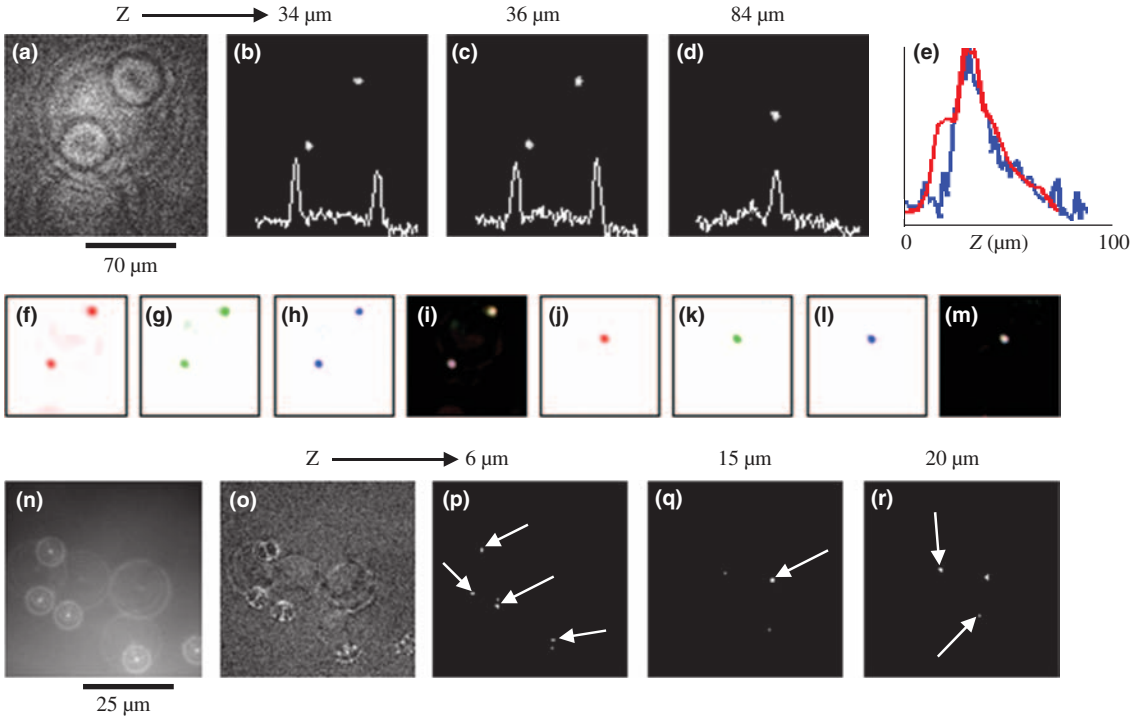

Fig. 18. FINCHSCOPE holography of polychromatic beads. (a) Magnitude of the complex hologram 6 μm beads. Images reconstructed from the hologram at z distances of (b) 34 μm, (c) 36 μm and (d) 84 μm. Line intensity profiles between the beads are shown at the bottom of panels b–d. (e) Line intensity profiles along the z axis for the lower bead from reconstructed sections of a single hologram (blue line) and from a widefield stack of the same bead (28 sections, red line). (f)–(h) Beads (6 μm) excited at 640, 555 and 488 nm with holograms reconstructed at planes b and (j–l) d. (i) and (m) are the combined RGB images for planes b and d, respectively. (n)–(r), Beads (0.5 μm) imaged with a 1.4-NA oil immersion objective: (n) holographic camera image; (o) magnitude of the complex hologram; (p–r), reconstructed image planes 6, 15 and 20 μm. Scale bars indicate image size.

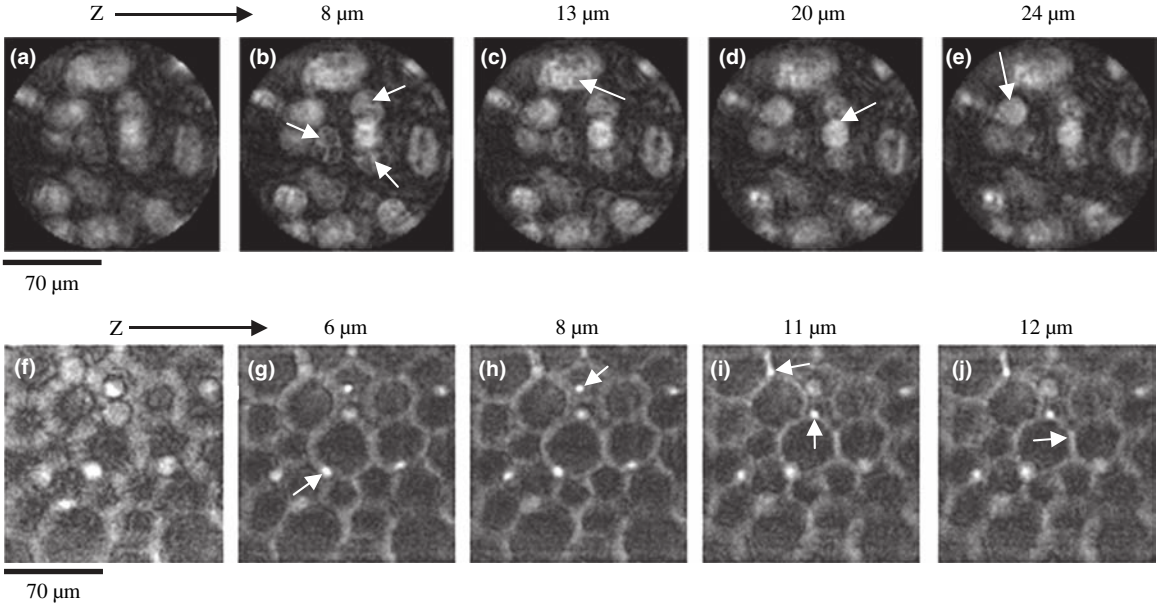

Fig. 19. FINCHSCOPE fluorescence sections of pollen grains and *Convallaria rhizom*. The arrows point to the structures in the images that are in focus at various image planes. (b)–(e), Sections reconstructed from a hologram of mixed pollen grains. (g)–(j), Sections reconstructed from a hologram of *Convallaria rhizom*. (a), (f), Magnitude of the complex holograms from which the respective image planes were reconstructed. Scale bars indicate image size.

5. DISCUSSION AND CONCLUSIONS

We have reviewed three different methods of generating incoherent digital Fresnel holograms. The homodyne scanning holography setup has some advantages over the previous designs of scanning holography. The main advantage is that the overall scanning time can be shorter than the case of heterodyne scanning holography. Also, the proposed system is more immune from noise than previous scanning holography systems because in the homodyne scanning holography, only frozen-in-time FZP patterns scan the object. However, the main limitation of scanning holography—the need for a 2-D scan—does exist in the homodyne version as well. In view of this limitation, the scanning holography, in all of its versions, is considered as the slowest method in capturing the scene among all three methods reviewed herein.

The second reviewed method, the DIMFH, is based on computer processing of multiple view projections. The projection capturing can be implemented with or without scanning. However in the non-scanning version, by using an MLA, the resolution of the system is sacrificed in order to get a hologram captured by a single camera shot. This limitation can be relieved by using a macrolens array and synthesizing the middle projection digitally. The main advantage of the DIMFH is that it is generated with a digital camera, operating in regular light conditions without beam interference at all. Thus, most disadvantages characterizing conventional holography, namely the need for a powerful, highly coherent laser and meticulous stability of the optical system are avoided. The implementation of the DIMFH for 3-D microscopy remains questionable, because among the three IDHs the DIMFH is the only one that observes the scene from more than one angular perspective. Using lens or camera arrays enable a single camera-shot imaging, which can be used for acquiring general moving bodies, no matter what the nature of the movement is. However, viewing a microscopic specimen from multiple view points is not a trivial task.

The third reviewed hologram, the FINCH, is actually recorded by an on-axis, single-channel, incoherent interferometer. Among all three methods this is the only one that inherently does not scan the object neither in the space nor in the time. Therefore, the FINCH can generate the hologram rapidly without sacrificing the system resolution. This system offers the feature of observing a complete volume from a hologram, potentially enabling objects moving quickly in three dimensions to be tracked. The FINCH technique shows great promise in rapidly recording 3-D information in any scene, independently of the illumination.

References and Notes

1. W. Lohmann and D. P. Paris, *Appl. Opt.* 6, 1739 **(1967)**.
2. U. Schnars, T. M. Kreis, and W. P. O. Juptner, *Opt. Eng.* 35, 977 **(1996)**.
3. J. Rosen, G. Indebetouw, and G. Brooker, *Opt. Express* 14, 4280 **(2006)**.
4. J. Rosen and G. Brooker, *Opt. Lett.* 32, 912 **(2007)**.
5. J. Rosen and G. Brooker, *Opt. Express* 15, 2244 **(2007)**.
6. J. Rosen and G. Brooker, *Nature Photon.* 2, 190 **(2008)**.
7. N. T. Shaked and J. Rosen, *Appl. Opt.* 47, D21 **(2008)**.
8. T.-C. Poon and A. Korpel, *Opt. Lett.* 4, 317 **(1979)**.
9. B. W. Schilling, T.-C. Poon, G. Indebetouw, B. Storrie, K. Shinoda, Y. Suzuki, and M. H. Wu, *Opt. Lett.* 22, 1506 **(1997)**.
10. T.-C. Poon, Optical Scanning Holography with MATLAB, Springer, New York **(2007)**.
11. T.-C. Poon, *J. Holography Speckle* 1, 6 **(2004)**.
12. G. Indebetouw, Y. Tada, J. Rosen, and G. Brooker, *Appl. Opt.* 46, 993 **(2007)**.
13. J. W. Goodman, Introduction to Fourier Optics, 2nd edn., McGraw-Hill, New York **(1996)**.
14. I. Yamaguchi and T. Zhang, *Opt. Lett.* 22, 1268 **(1997)**.
15. N. T. Shaked and J. Rosen, *J. Opt. Soc. Am. A* 25, 2129 **(2008)**.
16. N. T. Shaked, G. Segev, and J. Rosen, *Opt. Express* 16, 17148 **(2008)**.
17. N. T. Shaked, B. Katz, and J. Rosen, *Opt. Lett.* 33, 1461 **(2008)**.
18. Y. Li, D. Abookasis, and J. Rosen, *Appl. Opt.* 40, 2864 **(2001)**.
19. D. Abookasis and J. Rosen, *JOSA A* 20, 1537 **(2003)**.
20. D. Abookasis and J. Rosen, *Appl. Opt.* 45, 6533 **(2006)**.
21. Y. Sando, M. Itoh, and T. Yatagai, *Opt. Lett.* 28, 2518 **(2003)**.
22. T. Yatagai, *Appl. Opt.* 15, 2722 **(1976)**.
23. N. T. Shaked, J. Rosen, and A. Stern, *Opt. Express* 15, 5754 **(2007)**.
24. B. Katz, N. T. Shaked, and J. Rosen, *Opt. Express* 15, 13250 **(2007)**.

Received: xx Xxxx xxxx. Revised/Accepted: xx Xxxx xxxx.